# Benefits and Limitations of using Several Piezoelectric Cantilever Elements for Harvesting Vibration Energy in Moving Freight Cars

Lucas D. Coelho, Túlio F. Moreira, and Moisés V. Ribeiro

***Abstract*— This paper investigates an energy harvester constituted by an array of $N$ piezoelectric cantilever elements to raise the power harvested from the vibration energy in moving freight cars. Firstly, the parallel array is considered since it is able to increase the output current using the same bridge rectifier. Secondly, it demonstrates that connecting a number of $N$ piezoelectric cantilever elements in the parallel configuration results in an upper bound to the harvested power, which the provided closed-form expressions predict. Lastly, it shows that numerical results obtained with closed-form expressions and simulations present a small discrepancy, confirming the precision of the deduced theoretical model.**

***Keywords*— Energy harvesting. Vibration. Piezoelectricity.**

## I. Introduction

Implementing monitoring and condition-based maintenance solutions for railway assets is crucial within the railway industry. These solutions enhance the safety and reliability of the railway system, as they facilitate the predictive detection of component failures [1]. One significant area of concern pertains to freight cars, where incidents of wagon derailment are still reported [2]. It is surmised that such derailments could potentially be mitigated through vigilant monitoring of causative factors, including damaged rails, wheel or axle failure, and non-uniform braking [3]. Hence, deploying robust monitoring systems is imperative, not only for detecting these failures but also for timely communication of these incidences, thereby averting derailments or other train faults.

An important challenge lies in the power supply for these monitoring systems. Freight cars, unlike locomotives, are not equipped with their own power sources. The power distribution from the locomotive to the freight cars presents limitations, suggesting using batteries to power the monitoring systems. However, frequent replacement due to the limited lifespan of batteries, compounded by the high cost associated with installing them in all freight cars within a train composition, makes this solution impractical. In this context, energy harvesting emerges as a viable, sustainable, and long-term alternative. The principle of energy harvesting revolves around converting environmental energy sources into electricity. These sources include solar, wind (natural and artificial), thermal, noise, and vibration energies.

Given the railway environment's propensity for dust and mechanical shocks, which can be hostile to fragile devices, vibrations have been identified as a promising energy source for energy harvesting [4]. This process, referred to as vibration energy harvesting (VEH), has been explored for both line side and onboard applications in the railway system [5]. Note that VEH typically employs piezoelectric, electromagnetic, or electrostatic devices to convert environmental energy into electricity [4], [5]. Such a device is referred to as an energy harvester (EH). For the EH to extract maximum power, it is crucial that its fundamental frequency matches with that of the excitation source [3]. In cases where there is a mismatch in frequency, the power harvested is markedly reduced, necessitating wide operational bandwidth, thereby enhancing power extraction.

Given that the energy harvested by a single EH unit can often be lower than the required amount, it is vital to consider the energy density and compactness of the EH when seeking to increase the power harvested per unit of area or volume. Piezoelectric elements display these characteristics and are frequently studied in this context [3]. Existing literature reveals that the design and function of harvesting circuits are typically explored in railway systems when a single piezoelectric device is employed for energy harvesting [2], [4], [5]. This paper explores the advantages of utilizing a EH based on a parallel-connected array of piezoelectric cantilever to power freight car monitoring systems, with wagon vibrations serving as a VEH source. We extend the model of a single piezoelectric cantilever component to represent an array of $N$ piezoelectric cantilever components and formulate closed-form expressions to calculate the voltage, current, and potential power for harvesting. The numerical analysis shows that these quantities increase proportionally by adding more piezoelectric components to the array up to a certain $N$ value. After this value, a cumulative capacitive effect resulting from the parallel combination of these components hinders system efficiency and consequently limits the number of piezoelectric cantilever components that can be effectively integrated into such an arrangement.

The rest of this paper is organized as follows. Section II describes the model for an EH based on a single piezoelectric cantilever element. Section III derives an EH based on $N$

This research was supported in part by Coordenação de Aperfeiçoamento de Pessoal de Nível Superior (CAPES) under Grant 001, Conselho Nacional de Desenvolvimento Científico e Tecnológico (CNPq) under grants 404068/2020-0 and 314741/2020-8, Fundação de Amparo à Pesquisa do Estado de Minas Gerais (FAPEMIG) under grants APQ-03609-17, TEC-PPM 00787-18, and APQ-04623-22, and Instituto Nacional de Energia Elétrica (INERGE).

Lucas D. Coelho, Túlio F. Moreira, and Moisés V. Ribeiro are with the Electrical Engineering Department of Federal University of Juiz de Fora e-mail addresses: {lucas.coelho, tulio.fernandes, mribeiro}@engenharia.ufjf.br.

piezoelectric cantilever elements, while Section IV analyzes numerical results. Concluding remarks are stated in Section V.

## II. Modeling an Energy Harvester based on a Single Piezoelectric Cantilever

The simplified model of the single degree of freedom (SDOF) piezoelectric harvester is shown in Fig. 1 (a). It provides a faithful description of the behavior of the cantilever structure near the first bending mode resonance [6]. On the other hand, Fig. 1 (b) shows the equivalent electric circuit for this model connected to a resistive load. Now, consider

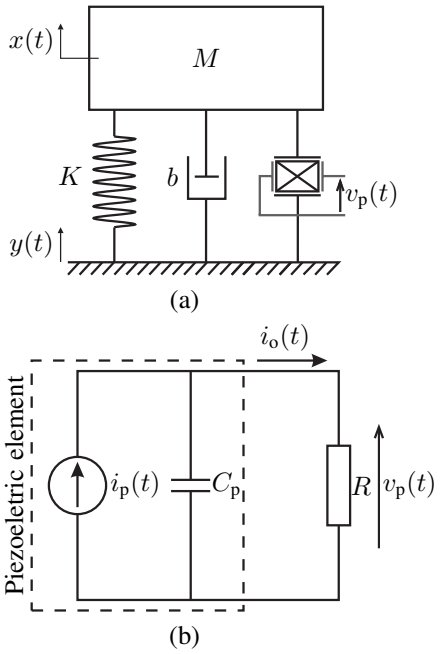


Fig. 1. SDOF piezoelectric vibration EH system connected to a resistive load: (a) Simplified SDOF harvester model. (b) Equivalent electric circuit of the model of the piezoelectric cantilever connected to a resistive load.

$z(t) = x(t) - y(t)$ (m) the relative displacement of the mass to the base and $v_{\rm p}(t)$ the voltage across the piezoelectric element, and apply Newton's second law of motion to the model in Fig. 1(a). The resulting differential equation is expressed by

$$M\frac{d^2z(t)}{dt^2} + b\frac{dz(t)}{dt} + Kz(t) = -M\frac{d^2y(t)}{dt^2} - \alpha v_{\rm p}(t), \quad (1)$$

in which $M$ (kg) is the total mass, $b$ (Ns/m) the mechanical damping coefficient, and $K$ (N/m) the total stiffness, and $\alpha$ (N/V or As/m) is the force factor. To relate the base excitation of the system ($y(t)$) to the piezoelectric output current ($i_{\rm o}(t)$), Kirchhoff's current law is applied in the equivalent electric circuit in Fig. 1(b). Consequently, we obtain the following differential equation:

$$\begin{aligned} i_{\rm o}(t) &= i_{\rm p}(t) - C_{\rm p}\frac{dv_{\rm p}(t)}{dt} \\ &= \alpha\frac{dz(t)}{dt} - C_{\rm p}\frac{dv_{\rm p}(t)}{dt}, \end{aligned} \quad (2)$$

where $i_{\rm p}(t)$ is the piezoelectric current and $C_{\rm p}$ (F) is the piezoelectric element capacitance. For the linear mass-spring-damper system showed in Fig. 1, the vibration of the base (the base excitation of the system) is modeled as $y(t) = Y\sin(\omega_r t + \phi)$, in which $\omega_r = 2\pi f_r$ and $f_r$ is the resonant frequency. Consequently, the displacement $z(t)$, the piezoelectric voltage $v_{\rm p}(t)$, and the current $i_{\rm o}(t)$ are also sinusoidal.

### A. Interfacing with a Full Bridge Rectifier

Microgeneration devices that supply energy to an electronic system need interface circuits that convert and regulate the generated power. For this purpose, the interface circuit most used in piezoelectric VEH devices is the full bridge rectifier shown in Fig. 2. Note that $C_{\rm s}$ is the capacitance of the smoothing capacitor, $R$ is the load resistance, and $v_{\rm rect}(t)$ is the voltage at the output of the rectifier. We assume that $RC_{\rm s} \gg 1/f_r$, and consequently $v_{\rm rect}(t) = V_{\rm rect}$.

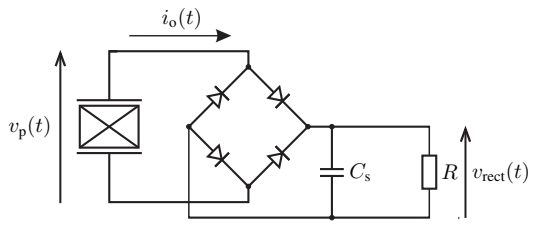


Fig. 2. Connecting the full bridge rectifier to the EH.

To obtain $V_{\rm rect}$ and the harvested power ($P_h$), it is necessary to integrate (2) in the range from $t_0$ to $t_0 + T/2$, where $T = 1/f_r$. This integration is expressed by

$$\int_{t_0}^{t_0+\frac{T}{2}} i_{\rm o}(t){\rm d}t = \int_{t_0}^{t_0+\frac{T}{2}} \alpha\frac{dz(t)}{dt}{\rm d}t - \int_{t_0}^{t_0+\frac{T}{2}} C_{\rm p}\frac{dv_{\rm p}(t)}{dt}{\rm d}t, \quad (3)$$

Note that (3) is solved for the case in which the oscillation of the rectified voltage wave is practically zero (i.e., $v_{\rm rect}(t) = V_{\rm rect}$). As the piezoelectric voltage $v_{\rm p}(t)$ is limited to $V_{\rm rect}$, then the average current flowing into the capacitor $C_S$ is zero [6]. Consequently,

$$\frac{\pi}{\omega}\frac{V_{\rm rect}}{R} = 2Z_{\max}\alpha - 2V_{\rm rect}C_{\rm p} \quad (4)$$

where $\omega = 2\pi f$ and $Z_{\max}$ is the value of the maximum relative displacement. Therefore, it is possible to determine the electrical variables at the resonant frequency, which is the frequency of interest in energy harvesting. The literature shows that $Z_{\max}$ has a known solution at $\omega = \omega_r$ [6], [7], which is given by

$$Z_{\max} = \frac{MA}{b\omega_r + \dfrac{2R\alpha^2}{(\omega_r RC_{\rm p} + \frac{\pi}{2})^2}\omega_r}, \quad (5)$$

where $A$ is the acceleration amplitude of the base excitation $y(t)$. Then,

$$V_{\rm rect} = \frac{\omega_r\alpha R}{\omega_r RC_{\rm p} + \frac{\pi}{2}}Z_{\max}, \quad (6)$$

and the current through the load resistance is given by

$$I_{\rm rect} = \frac{\alpha\omega_r}{\omega_r RC_{\rm p} + \frac{\pi}{2}}Z_{\max}. \quad (7)$$

The harvested power at the output of the full bridge rectifier is given by

$$P_{\mathrm{h}} = \frac{R\alpha^2\omega_r^2}{\left(\omega_r RC_{\mathrm{p}} + \frac{\pi}{2}\right)^2} Z_{\max}^2. \tag{8}$$

## III. Modeling an Energy Harvester based on $N$ Piezoelectric Cantilever

As a single piezoelectric cantilever EH provides a limited amount of energy, the use of an array connecting $N$ of them can increase the capacity to harvest energy. The parallel configuration is straightforward, simple, and cost-effective for increase current connecting $N$ piezoelectric cantilevers because only one full bridge rectifier can be used to harvest energy from them. This section extends the results presented in Section II to the parallel configuration of $N$ piezoelectric cantilevers. To do so, we assume that the $N$ piezoelectric cantilevers are fixed to the same freight car, and consequently, they are subjected to the same base excitation or displacement ($y(t)$) and, consequently, they generate individually the same voltage, $v_{\mathrm{p}}(t)$, at their output terminals.

### A. Model Description

Fig. 3 shows the block diagram for the parallel connection of $N$ piezoelectric cantilever elements, represented by $N$ SDOF models coupled in parallel, to a full bridge rectifier. For the sake of simplicity, the full bridge rectifier shown in Fig. 2 is adopted.

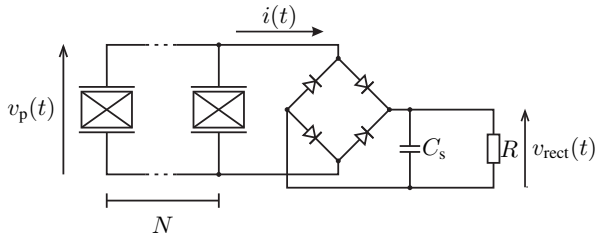


Fig. 3. Equivalent electric circuit for the array of $N$ piezoelectric cantilever elements coupled to a full bridge rectifier.

Note that (1) remains unchanged for each piezoelectric cantilever EH; however, the same does not occur for (2). Considering the principle of superposition, the application of Kirchhoff's law of current in the equivalent electric circuit showed in Fig. 3 leads to $i(t) = \sum_{n=1}^{N} i_n(t)$, where $i_n(t)$ is the current delivered by the $n^{\text{th}}$ piezoelectric element and equal to $i_{\mathrm{o}}(t)$. Then,

$$i(t) = N\alpha\frac{dz(t)}{dt} - NC_{\mathrm{p}}\frac{dv_{\mathrm{p}}(t)}{dt}. \tag{9}$$

Integrating (9) in the interval delimited by $t_0$ to $t_0 + T/2$, and considering the $Z_{\max}$ given by (5), and $v_{\mathrm{rect}}(t) = V_{\mathrm{rect}}$, results in

$$\frac{\pi}{\omega_r}\frac{V_{\mathrm{rect}}}{R} = 2N\alpha Z_{\max} - 2NC_{\mathrm{p}}V_{\mathrm{rect}}. \tag{10}$$

Then,

$$V_{\mathrm{rect}} = \frac{RN\alpha\omega_r}{\omega_r RNC_{\mathrm{p}} + \frac{\pi}{2}} Z_{\max}, \tag{11}$$

and the current over the load resistance is given by

$$I_{\mathrm{rect}} = \frac{N\alpha\omega_r}{\omega_r RNC_{\mathrm{p}} + \frac{\pi}{2}} Z_{\max}. \tag{12}$$

The harvested power is given by

$$P_{\mathrm{h}} = \frac{RN^2\alpha^2\omega_r^2}{\left(\omega_r RNC_{\mathrm{p}} + \frac{\pi}{2}\right)^2} Z_{\max}^2. \tag{13}$$

Consequently, the array of $N$ piezoelectric cantilever elements in the parallel configuration can be modeled by an equivalent current source equal to $i_{\mathrm{p,e}} = Ni_{\mathrm{p}}(t)$ in parallel to the equivalent capacitance equal to $C_{\mathrm{p,e}} = NC_p$. Consequently, the capacitance $C_{\mathrm{p,e}}$ drains much of the equivalent current as $N$ increases. For that reason, there is an upper bound (UB) in $V_{\mathrm{rect}}$, $I_{\mathrm{rect}}$, and $P_{\mathrm{h}}$ values when $N \to \infty$. The UB for $V_{\mathrm{rect}}$ is given by

$$V_{\mathrm{rect,UB}} = \lim_{N\to\infty} \frac{RN\alpha\omega_r}{\omega_r RNC_{\mathrm{p}} + \frac{\pi}{2}} Z_{\max} \tag{14}$$

$$= \frac{\alpha}{C_{\mathrm{p}}} Z_{\max}. \tag{15}$$

Consequently, the UB for $I_{\mathrm{rect}}$ is given by

$$I_{\mathrm{rect,UB}} = \frac{\alpha}{RC_{\mathrm{p}}} Z_{\max}. \tag{16}$$

Finally, the UB for the harvested power is expressed as

$$P_{\mathrm{h,UB}} = \frac{\alpha^2}{RC_{\mathrm{p}}^2} Z_{\max}^2. \tag{17}$$

## IV. Numerical Analysis

This section discusses numerical results obtained with the closed-form expressions and the simulations carried out with the LTspice software when the array of $N \in \{1, 2, ..., 10^3\}$ piezoelectric cantilever elements are connected in the parallel configuration. To obtain these numerical results, we followed [7] to define the parameters of the SDOF model for the piezoelectric cantilever element. In this sense, the resonant frequency equal to 12 Hz, $M = 2.20 \times 10^{-2}$ kg, $K = 1.25 \times 10^2$ N/m, and $b = 1.54 \times 10^{-1}$ Ns/m, and $A = 3.46$ m/s$^2$. Moreover, the electrical parameters associated with one piezoelectric element, namely the force factor and piezoelectric capacitance, are given by $\alpha = 1.52 \times 10^{-3}$ N/V and $C_{\mathrm{p}} = 1.89 \times 10^{-8}$ F. Also, the full bridge rectifier uses $C_{\mathrm{s}} = 22 \times 10^{-6}$ F for a relatively small ripple and the load resistance of $R = 97.40 \times 10^3$ Ω, which is set to maximize the power transfer. Table I lists all these values.

### A. Numerical Results: Closed-Form Expressions

Table II presents the voltage, current, and power obtained with the closed-form expressions while increasing the number ($N$) of piezoelectric elements in the array. These values were obtained using (11), (12), and (13). In general, for $N \leq 100$, there is a considerable increase in $V_{\mathrm{rect}}$, $I_{\mathrm{rect}}$, and $P_{\mathrm{h}}$. However, the increase starts to reduce for values of $N \geq 100$, and for $N \geq 1000$, the increase becomes irrelevant. When $N \to \infty$, we obtain $V_{\mathrm{rect,UB}}$, $I_{\mathrm{rect,UB}}$, and $P_{\mathrm{h,UB}}$, given by (15), (16), and (17), respectively.

TABLE I
PARAMETERS OF THE SDOF MODEL.

| Parameter | Values | Units |
|---|---|---|
| $M$ | $2.20 \times 10^{-2}$ | kg |
| $b$ | $1.54 \times 10^{-1}$ | Ns/m |
| $K$ | $1.25 \times 10^{2}$ | N/m |
| $C_{\text{p}}$ | $1.89 \times 10^{-8}$ | F |
| $C_{\text{s}}$ | $2.2 \times 10^{-5}$ | F |
| $\alpha$ | $1.52 \times 10^{-3}$ | N/V |
| $R$ | $97.403 \times 10^{3}$ | $\Omega$ |
| $A$ | 3.463 | m/s$^2$ |

For instance, for $N = 100$, the voltage, current, and power generated are equal to 237.07 V, 2.43 mA, and 577.02 mW, respectively, which is much greater than the values of 21.42 V, 0.22 mA, and 4.71 mW, yielded with $N = 1$. But, with $N = 1000$, the values of $V_{\text{rect}}$, $I_{\text{rect}}$, and $P_{\text{h}}$ are equal to 260.95 V, 2.68 mA, and 699.13 mW, which does not show much gain from using $N = 100$ piezoelectric elements. In such way, if $N \to \infty$, these values converge to 263.91 V, 2.71 mA, and 715.05 mW.

TABLE II
NUMERICAL RESULTS OBTAINED WITH CLOSED-FORMS.

| $N$ | $V_{\text{rect}}$ (V) | $I_{\text{rect}}$ (mA) | $P_{\text{h}}$ (mW) |
|---|---|---|---|
| 1 | 21.4214 | 0.2199 | 4.7111 |
| 2 | 39.6263 | 0.4068 | 16.1211 |
| 3 | 55.2886 | 0.5676 | 31.3833 |
| 10 | 123.7853 | 1.2709 | 157.3134 |
| 100 | 237.0725 | 2.4339 | 577.0188 |
| 1000 | 260.9548 | 2.6791 | 699.1307 |
| $\infty$ | 263.9088 | 2.7095 | 715.0485 |

### B. Numerical Results: Simulations

The numerical simulations of the equivalent electric circuit in Fig. 3 were carried out assuming that each of the $N$ piezoelectric cantilever elements is modeled as an equivalent current source parallel to an equivalent capacitor. Therefore, we assume the equivalent current source and capacitance are equal to $i_{\text{p,e}}(t)$ and $C_{\text{p,e}}$, respectively. The used parameters are in Table I, and the diode is the 1N4148. Since the $C_{\text{s}}$ chosen is finite, a ripple remains in the rectified voltage and current. Thus, the average of these values was calculated over the half period, and it will be differently marked with an overline on the variable, i.e., $\overline{V}_{\text{rect}}$, $\overline{I}_{\text{rect}}$, and $\overline{P}_{\text{h}}$.

Numerical results for distinct values of $N$ are listed in Table III. According to this table, for $N = 100$, $\overline{V}_{\text{rect}}$, $\overline{I}_{\text{rect}}$, and $\overline{P}_{\text{h}}$ are equal to 234.59 V, 2.41 mA, and 565.03 mW, respectively, which is greater than the values of 21.37 V, 0.22 mA, and 4.69 mW, yielded with $N = 1$. But, with $N = 1000$, the values of $\overline{V}_{\text{rect}}$, $\overline{I}_{\text{rect}}$, and $\overline{P}_{\text{h}}$ are equal to 257.49 V, 2.64 mA, and 680.70 mW, which also does not show much gain from using $N = 100$. Overall, the simulation results show a behavior coherent to the results obtained with the closed-form expressions.

TABLE III
NUMERICAL RESULTS OBTAINED WITH SIMULATIONS.

| $N$ | $\overline{V}_{\text{rect}}$ (V) | $\overline{I}_{\text{rect}}$ (mA) | $\overline{P}_{\text{h}}$ (mW) |
|---|---|---|---|
| 1 | 21.3675 | 0.2194 | 4.6874 |
| 2 | 39.5122 | 0.4057 | 16.0285 |
| 3 | 55.1127 | 0.5658 | 31.1841 |
| 10 | 123.1810 | 1.2647 | 155.7830 |
| 100 | 234.5940 | 2.4085 | 565.0290 |
| 1000 | 257.4880 | 2.6435 | 680.6950 |

### C. Numerical Results: A Comparison

This subsection presents a comparative analysis of numerical results, derived from both closed-form expressions and simulations, pertaining to the voltage, current, and harvested power at the load resistance terminals. This analysis considers an array size, denoted by $N$, that ranges from 1 to $10^3$.

- **Voltage**. The voltage across the load resistance versus $N$ is shown in Fig. 4 (a). Note that the numerical results obtained with closed-form expressions and simulations present a small discrepancy even when $N$ is large. According to Tables IV, the difference between both values varies from $0.25\%$ and $1.33\%$ when $N$ goes from 1 to $10^3$, respectively.

TABLE IV
COMPARISON IN TERMS OF VOLTAGE

| $N$ | $V_{\text{rect}}$ (V) | $\overline{V}_{\text{rect}}$ (V) | Absolute diff. | Relative diff. |
|---|---|---|---|---|
| 1 | 21.4214 | 21.3675 | 0.0539 | 0.25% |
| 2 | 39.6263 | 39.5122 | 0.1141 | 0.29% |
| 3 | 55.2886 | 55.1127 | 0.1759 | 0.32% |
| 10 | 123.7853 | 123.1810 | 0.6043 | 0.49% |
| 100 | 237.0725 | 234.5940 | 2.4785 | 1.05% |
| 1000 | 260.9548 | 257.4880 | 3.4668 | 1.33% |

- **Current**. The current through the load resistance versus $N$ is shown in Fig. 4 (b). Note that the numerical results obtained with closed-form expressions and simulations present a small discrepancy. The difference between them varies from $0.25\%$ and $1.33\%$ when $N$ goes from 1 to $10^3$, respectively, as it can be inferred from the values in Table V. Note that the absolute difference is less than for voltage values due to the high value of the used load resistance.
- **Power**. The harvested power by the load resistance versus $N$ is shown in Fig. 4 (c). Similar to voltage and current, numerical results obtained with closed-form expressions and simulations present a small discrepancy. The difference between them varies from $0.50\%$ and $2.64\%$ when $N$ goes from 1 to $10^3$, respectively, as

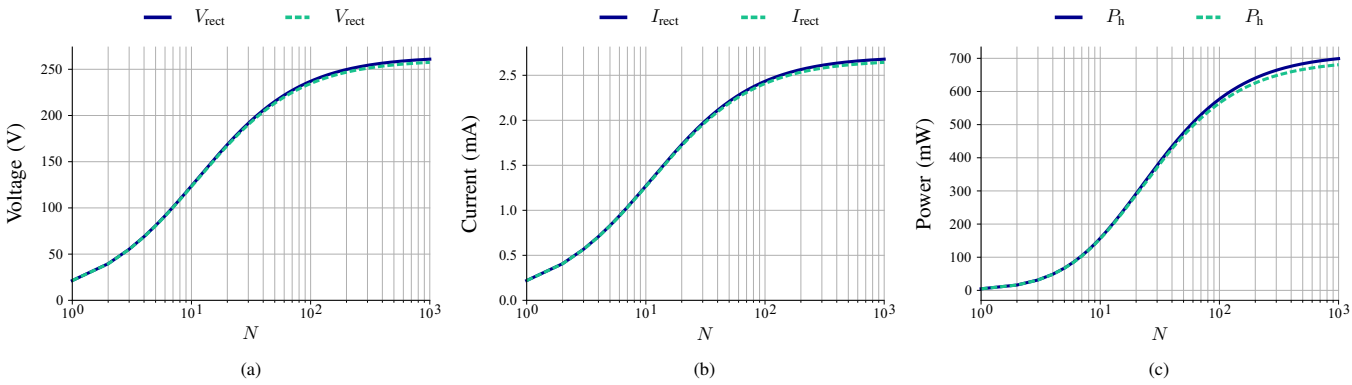


Fig. 4. Performance comparison: (a) voltage, (b) current, and (c) harvested power. Numerical results for closed-form expressions (blue continuous line) and simulations (green dashed line).

TABLE V
COMPARISON IN TERMS OF CURRENT

| $N$ | $I_{\text{rect}}$ (mA) | $\overline{I}_{\text{rect}}$ (mA) | Absolute diff. | Relative diff. |
|---|---|---|---|---|
| 1 | 0.2199 | 0.2194 | 0.0006 | 0.25% |
| 2 | 0.4068 | 0.4057 | 0.0012 | 0.29% |
| 3 | 0.5676 | 0.5658 | 0.0018 | 0.32% |
| 10 | 1.2709 | 1.2647 | 0.0062 | 0.49% |
| 100 | 2.4339 | 2.4085 | 0.0254 | 1.05% |
| 1000 | 2.6791 | 2.6435 | 0.0356 | 1.33% |

TABLE VI
COMPARISON IN TERMS OF HARVESTED POWER

| $N$ | $P_{\text{h}}$ (mW) | $\overline{P}_{\text{h}}$ (mW) | Absolute diff. | Relative diff. |
|---|---|---|---|---|
| 1 | 4.7111 | 4.6874 | 0.0236 | 0.50% |
| 2 | 16.1211 | 16.0285 | 0.0926 | 0.57% |
| 3 | 31.3833 | 31.1841 | 0.1992 | 0.63% |
| 10 | 157.3134 | 155.7830 | 1.5304 | 0.97% |
| 100 | 577.0188 | 565.0290 | 11.9898 | 2.08% |
| 1000 | 699.1307 | 680.6950 | 18.4357 | 2.64% |

presented in Table VI. The error is slightly larger than voltage and current due to uncertainty propagation.

The numerical results from closed-form expressions demonstrate high agreement with those obtained through simulations for $N$ ranging from 1 to $10^3$. The discrepancy between the two sets of results is acceptably small, at less than 3%. Also, when considering smaller $N$ values, there is a substantial increase in voltage and current; however, as $N$ increases further, the growth in these quantities becomes marginal.

## V. CONCLUSIONS

This paper has investigated an energy harvester constituted by an array of $N$ piezoelectric cantilever elements with the aim of raising the power harvested from the vibration energy observed in moving freight cars. Initially, the findings suggest that the most effective configuration for this array is parallel, primarily because all piezoelectric cantilever elements share a single full bridge rectifier, which reduces cost. Subsequently, through the use of closed-form expressions, we have substantiated the existence of an upper bound to the power that can be harvested. Furthermore, our numerical results reveal a negligible increase in the harvested power for $N \geq 100$. It is also noteworthy that the numerical results, derived from both closed-form expressions and simulations, exhibit minimal discrepancy, thereby underscoring the accuracy of our theoretical model.

## REFERENCES

[1] V. J. Hodge, S. O'Keefe, M. Weeks, and A. Moulds, "Wireless sensor networks for condition monitoring in the railway industry: A survey," *IEEE Transactions on Intelligent Transportation Systems*, vol. 16, no. 3, pp. 1088–1106, Jun. 2015.

[2] E. Bernal, M. Spiryagin, and C. Cole, "Onboard condition monitoring sensors, systems and techniques for freight railway vehicles: A review," *IEEE Sensors Journal*, vol. 19, no. 1, pp. 4–24, Jan. 2019.

[3] M. Valente Lopes, J. Eckert, T. Martins, and A. Santos Jr, "Optimizing strain energy extraction from multi-beam piezoelectric devices for heavy haul freight cars," *Journal of the Brazilian Society of Mechanical Sciences and Engineering*, vol. 42, Jan. 2020.

[4] A. Hosseinkhani, D. Younesian, P. Eghbali, A. Moayedizadeh, and A. Fassih, "Sound and vibration energy harvesting for railway applications: A review on linear and nonlinear techniques," *Energy Reports*, vol. 7, pp. 852–874, Nov. 2021.

[5] L. Qi, H. Pan, Y. Pan, D. Luo, J. Yan, and Z. Zhang, "A review of vibration energy harvesting in rail transportation field," *iScience*, vol. 25, no. 3, p. 103849, Mar. 2022.

[6] E. Lefeuvre, A. Badel, C. Richard, and D. Guyomar, "Piezoelectric energy harvesting device optimization by synchronous charge extraction," *Journal of Intelligent Material Systems and Structures*, vol. 16, pp. 865–876, Oct. 2005.

[7] D. Guyomar, G. Sebald, and H. Kuwano, "Energy harvester of 1.5 $\text{cm}^3$ giving output power of 2.6 mW with only $1g$ acceleration," *Journal of Intelligent Material Systems and Structures*, vol. 22, no. 5, pp. 415–420, Mar. 2011.